CHAPTER 102

BREAKING WAVE FORCES ON A LARGE DIAMETER CELL

Akira Watanabe
Lecturer
and
Kiyoshi Horikawa
Professor

Department of Civil Engineering
University of Tokyo
Tokyo, Japan

ABSTRACT

Experiments have been carried out by using non-breaking waves and breaking waves to investigate the wave forces on a vertical circular cell located in the shallow water. Based on the experimental data, the drag coefficient and the inertia coefficient of a circular cylinder and the curling factor of breaking waves are estimated, and the computation methods of wave forces are examined. As a result, it is shown that the phase lag of inertia forces behind the accelerations of water particles should be considered for the estimation of the drag coefficient as well as the inertia coefficient. In addition the previous formula of the maximum breaking wave forces acting on a cell or a pile is revised by introducing the effects of the above-mentioned phase lag and another phase difference, both of which are functions of the ratio of the cell diameter to the wave length. It is confirmed that the proposed formula is applicable even to the large cell with the diameter comparable to the wave length.

INTRODUCTION

Many studies have been done on the impulsive pressures acting on a vertical wall, but there has been very little investigation of breaking wave forces on a cell-type structure. The breaking wave forces should be taken into consideration all the same in the design of pile-type or cell-type structures in nearshore area, because breaking waves cause extreme shock pressures on a cell structure as

well as on a vertical wall.

Hall(1958) reported experimental data of the breaking wave forces on a circular pile located on a sloping beach. Goda *et al.*(1966) applied von Kármán's theory on the impact of the seaplane float during its landing to the estimation of the impact force of breaking waves, and they proposed the computation method of the impulsive breaking wave forces acting on the total length of a pile. It was a great step in the present problem, but whether their formula can be applied to the large diameter cell has been uncertain.

In the present paper it is shown that the ratio of the cell diameter to the wave length is one of the important parameters for the estimation of wave forces in the range of wave conditions from non-breaking to after-breaking, and a revised formula for the maximum breaking wave force acting on a large diameter cell is proposed.

PREVIOUS STUDIES OF WAVE FORCES ACTING ON A CIRCULAR CYLINDER

Non-breaking Wave Forces

The total force F_T exerted on a vertical circular pile by non-breaking waves is usually expressed as the sum of the drag force and the inertia force in the following form:

$$F_T = \frac{w_o}{2g} D \int_{-h}^{\eta} C_D u|u|dz + \frac{w_o}{g} \frac{\pi D^2}{4} \int_{-h}^{\eta} C_M \dot{u} dz \qquad (1)$$

where w_o is the specific weight of water, g is the acceleration of gravity, D is the pile diameter, u is the horizontal velocity of water particles, $\dot{u}$ is the horizontal acceleration of water particles, η is the surface elevation above the still water level, h is the water depth, and C_D and C_M are called the drag coefficient and the inertia coefficient respectively.

If the phase difference between the water particle acceleration and the inertia force as well as between the velocity and the drag force is assumed to be negligibly small, the total wave force F_T and the maximum value $(F_T)_{max}$ are represented as follows:

$$F_T(\theta) = (F_D)_{max}\sin^2\theta + (F_M)_{max}\cos\theta \qquad (2)$$

$$\left.\begin{aligned}(F_T)_{max} &= (F_D)_{max} + (F_M)^2_{max}/4(F_D)_{max} \quad \text{for } 2(F_D)_{max} > (F_M)_{max} \\ &= (F_M)_{max} \quad \text{for } 2(F_D)_{max} < (F_M)_{max}\end{aligned}\right\} \qquad (3)$$

where $(F_D)_{max}$ and $(F_M)_{max}$ are the maximum values of the drag force and the inertia force respectively, and θ is the phase angle which is zero at the instant when the water surface crosses the still water level upwards.

Breaking Wave Forces

When breaking waves act on a pile, an impact force is added to the drag force and the inertia force. Goda *et al.*(1966) assumed that the impact force is the result of the change in momentum of the water mass of a vertical wave front which has the height of $\lambda\eta_c$ and the velocity equal to breaking wave celerity c_b, and they expressed the total impact force on a pile as follows:

$$F_I = w_o D H_b^2 K_B \lambda (1 - t/\tau_B) \qquad 0 \leq t \leq \tau_B \qquad (4)$$

$$\left.\begin{aligned}K_B &= \pi c_b^2 \eta_c / 2g H_b^2 \ : \ \text{Impulsive force factor} \\ \tau_B &= D/2c_b \ : \ \text{Duration time of impact force}\end{aligned}\right\} \qquad (5)$$

where H_b is the breaking wave height, η_c is the crest height above the still water level and λ is the curling factor of breaking waves. The values of the curling factor were determined experimentally and were presented as a function of the bottom slope and the relative depth at the breaking point.

Since the duration time of the impact force is very short, the resultant stress in a structure or the measured value of the impact force depends not only upon the magnitude of the impact force itself, but also upon the natural frequency of the structure. Goda *et al.* have simplified the actual pile as a single-degree of freedom oscillatory system, and have shown that the effective impact force on an actual pile $(F_I)_e$ is expressed by $(F_I)_e = X_{max} F_I$, where X_{max} is the impact response factor which depends on both the duration time τ_B and the natural frequency as a func-

tion of their product.

By assuming that the wave profile ahead the vertical wave front is approximated as $\eta = \eta_c \sin\theta$, the phase angle θ_B at the collision of wave front can be given by $\sin^{-1}(1-\lambda)$, because $\eta=(1-\lambda)\eta_c$ at the phase of breaking. Therefore the drag force and the inertia force which should be added to the above impact force are expressed as follows:

$$(F_D)_B = (F_D)_{max}(1-\lambda)^2 \qquad (6)$$

$$(F_M)_B = (F_M)_{max}\sqrt{1-(1-\lambda)^2} \qquad (7)$$

Goda *et al.* have confirmed the validity of their model by means of their experimental data for four test piles. It has been, however, uncertain whether their formula is applicable to the large diameter cell or not.

EXPERIMENTAL APPARATUS AND PROCEDURES

Wave Force Measuring Apparatus

In order to examine the applicability of the above-mentioned formulae to the large diameter cell, the authors performed laboratory experiments for two test cells with the diameters of 13 cm and 50 cm respectively.

The force measuring apparatus for the cell with the diameter of 50 cm is sketched out in Fig. 1. The test cell made of duralumin is supported by slide bearings and is able to move parallel to the wave direction with very little friction. The wave force acting on this test cell is transmitted to two strain plates upper and lower (300 mm center to center), through steel rods. Therefore we can determine the total wave force and the height of action point by measuring strains of these strain plates. The strain plates and the slide bearings are fixed on the foundation, which has sufficiently high rigidity and large weight and is bolted to the base buried in the concrete bottom.

The test cell with the diameter of 13 cm is structurally similar to the one shown in Fig. 1. Table 1 shows the characteristics of these test cells.

Experimental Procedures

A wave basin, 40 m long, 25 m wide, from 0.6 to 1.1 m deep, was used for the present experiments (Fig. 2). Training walls were placed in this basin in order to divide the width of wave channel at 6 m, and a sloping bottom of 1 to 30 was settled between them.

The still water depth at the front of the cell was always kept 20 cm, and the wave period was varied from 1.0 to 2.0 sec at 0.25 sec intervals. In order to investigate also the values of the inertia coefficient and the drag coefficient for the large diameter cell, the wave height was also changed from about 2 cm to after-breaking condition for each wave period. The experimental wave conditions are shown in Table 2.

The incident wave height and the wave height at the location of the cell were measured by resistance type wave gages with two parallel copper wires. Another wave gage was settled at the location of 60 to 100 cm ahead the cell in order to measure the wave celerity. In addition, six current meters of miniature propeller type were set on a vertical beam at intervals of 5 cm so as to measure the distributions of horizontal velocities. A small light source and a photo-transistor are mounted on these current meters, and when the propeller rotates, the four blades of it cut off the light beam; thus each rotation of the propeller produces four pulse signals. The orbital velocities under wave crest are supposed to be purely horizontal, so we can evaluate these maximum orbital velocities from the closest time interval of pulse signals by using the calibration curve gained by the uniform flow perpendicular to the meters.

The breaker forms were observed to be spilling type for the wave period less than 1.5 sec and plunging type for the period greater than 1.75 sec. It was difficult to detect breaker heights by the wave gage on account of fluctuations of the breaking position, but the mean values of recorded breaker heights coincided nearly to the evaluated ones from the new breaker index proposed by Goda(1970). In the present analysis the authors employed this breaker index for the evaluation of the breaker height H_b, the breaker depth h_b, and the crest height above the bottom Y_b.

Figure 3 shows one example of breaking wave force on the large diameter cell. A typical impact force with

duration time of about 0.2 sec can be recognized.

EXPERIMENTAL RESULTS

Wave Celerity and Horizontal Velocity

The wave celerities were estimated from the wave records obtained by two wave gages located with interval from 60 to 100 cm nearby the test cell. The ratio of this actual wave celerity c to the one given by the small amplitude wave theory c_A is shown in Fig. 4 in relation to the steepness of deep water waves.

According to the pulse records of orbital velocities, the maximum horizontal velocities were observed to occur almost under the wave crest except in the vicinity of the bottom where the maximum velocities lag behind the wave crest about 0.08 sec at maximum. Ignoring these lags, the authors have chosen the maximum values at each elevation as the maximum velocities under the wave crest.

Goda(1964) has expressed this maximum velocities u_{max} by the product of orbital velocities of the small amplitude wave theory and a velocity factor K which represents the finite amplitude effect in the following form:

$$\left.\begin{aligned} u_{max}(z) &= K\frac{\pi H}{T}\cdot\frac{\cosh k(h+z)}{\sinh kh} \\ K &= \sqrt{1+\alpha\left(\frac{H}{h}\right)^{1/2}\cdot\left(1+\frac{z}{h}\right)^{3}}\ , \quad k=\frac{2\pi}{L_A} \end{aligned}\right\} \qquad (8)$$

where L_A is the wave length given by the small amplitude wave theory, and a factor α is a function of only the relative water depth h/L_A. Goda has calculated the values of α by using the Iversen's breaker index on the assumption that the horizontal velocities at the breaker crest, that is $u_{max}(Y_b-h)$ in Eq.(8), should be equal to the breaking wave celerity c_b. The values of α for the present condition have been calculated by using the Goda's new breaker index and the measured breaking wave celerity, and are shown in Table 3.

Figure 5 shows the comparison of the vertical distributions of the measured velocities and the values calculated with the use of Eq.(8) and the factor α given in

Table 3. The calculated values exceed the measured ones in the neighborhood of the wave crest as the wave height increases, but the difference between them is not so great as a whole. It is also similar in the cases of other wave periods.

The Inertia Coefficient

A number of laboratory investigations have been conducted in order to determine the magnitudes of the inertia coefficient and the drag coefficient. Most of these studies are depending on the expression of the total force shown in Eq.(2); in other words, they are based on the assumption that is sufficiently small the phase difference between the water particle acceleration and the inertia force as well as between the particle velocity and the drag force.

MacCamy and Fuchs(1954) have examined the inertia force on a single pile by a diffraction approach. According to their investigation, the inertia force $F_M(\theta)$ is given by

$$F_M(\theta) = (F_M)_{max}\cos(\theta-\varepsilon)$$

$$= \frac{w_o}{g}\frac{\pi D^2}{4}\hat{C}_M\int_{-h}^{\eta}\dot{u}_{max}\cos(\theta-\varepsilon)\,dz \qquad (9)$$

$$\hat{C}_M = \frac{4}{\pi\delta^2\sqrt{J_1'(\delta)^2+Y_1'(\delta)^2}}, \quad \varepsilon = \tan^{-1}\frac{J_1'(\delta)}{Y_1'(\delta)}, \quad \delta = \frac{\pi D}{L} \qquad (10)$$

which shows that the inertia force lags behind the particle acceleration by the phase angle ε, and that this phase lag and inertia coefficient $\hat{C}_M$ depend on the ratio of the pile diameter D to the wave length L. These quantities are presented by solid lines in Fig. 6.

By introducing the phase lag ε and by assuming that there is no phase difference between the horizontal velocity and the drag force, Eq.(2) for the total force is modified to the following equation:

$$F_T(\theta) = (F_D)_{max}\sin^2\theta + (F_M)_{max}\cos(\theta-\varepsilon) \qquad (11)$$

Therefore the estimation of the inertia coefficients through the relation $F_T(0)=(F_M)_{max}$, which is deduced from

Eq.(2), has a risk of underestimation of them.

The inertia coefficients derived from the measured non-breaking wave forces are plotted in Fig. 6. The quantities $(C_M)_o$ are based on the relation $F_T(0)=(F_M)_{max}$ and show a tendency to be less than the theoretical values given by Eq.(10). In the case of the large cell with the diameter of 50 cm, since the values of $(F_D)_{max}$ are only 10 per cent of $(F_M)_{max}$ and the phase difference ε is about 20 degrees at the most, so the error due to neglect of the drag force in the neighborhood of the phase $\theta=\varepsilon$ is less than 1 per cent; hence $(F_T)_{max}$ is supposed to be equal to $(F_M)_{max}$. The quantities $(C_M)_T$ in Fig. 2 are thus evaluated from the maximum total wave force $(F_T)_{max}$, and they have a tendency to be slightly greater than the theoretical values. This fact seems to be caused by the reason that the accelerations of water particles have been estimated by the small amplitude wave theory. In the case of the diameter of 13 cm, since the drag force is not so small, the values of $(C_M)_T$ have not been calculated.

The Drag Coefficient

The drag coefficients are usually estimated on the basis of the assumption that the drag force reaches the maximum and no inertia force is present under the wave crest ($\theta=\pi/2$). Equation(11) means, however, the inertia force is not zero at the phase $\theta=\pi/2$. In this paper the authors have estimated the values of the drag coefficient from the maximum drag force $(F_D)_{max}$ given by

$$(F_D)_{max} = F_T(\pi/2+\varepsilon)/\cos^2\varepsilon \qquad (12)$$

and from the measured velocities.

The drag coefficients C_D thus computed are shown by solid circles and solid triangles in Fig. 7 in relation to Reynolds number $R_e = u_o D/\nu$, where u_o is orbital velocity under the wave crest at the still water level computed from Eq.(8). These values C_D agree well with the steady flow data expressed as NPL curve given by Goldstein. The values C_D' in the same figure are the drag coefficients evaluated on the basis of the relation $(F_D)_{max} = F_T(\pi/2)$ without the phase difference ε. Figure 7 implies that the phase lag of the inertia force should be considered for the estimation of the drag coefficient as well as the inertia coefficient.

The Curling Factor of Breaking Waves

The curling factor λ of breaking waves is defined in the above-mentioned impact force model as the ratio of the vertical wave front height to the crest height above the still water level. But the vertical wave front is a hypothetical idea, and it is difficult to estimate this factor λ by using the actual shape of the breaking wave front. In practice λ is to be determined from the impact force records through the following equation;

$$(F_I)_e = X_{max} \frac{\pi}{2} \frac{w_o}{g} D c_b^2 \lambda \eta_c \qquad (13)$$

which is the expression of the maximum value of effective impact force reduced from Eqs.(4) and (5). In the present analysis the authors have regarded the peak value above the starting value of the sharp spike in the impulsive force records as the maximum impact force $(F_I)_e$ as shown in Fig. 8. The impact response factor X_{max} has been given by Goda *et al.*(1966) as a function of the product of impact duration time τ_B, which can be calculated from Eq.(5) by using the measured wave celerity c_b, and natural frequency of a cell in water.

Figure 9 shows the relation between the curling factor and the relative water depth h_b/L_A for the present case of the bottom slope of 1 to 30 together with the data given by Goda *et al.* for the bottom slope of 1 to 10 and 1 to 100 respectively. The magnitudes of the curling factor show a decreasing trend with increasing relative depth or with decreasing bottom slope. This is well understood as the effect of change of the breaker type from plunging to spilling type.

COMPARISON OF MEASURED WAVE FORCES AND CALCULATED ONES

Computation Methods of Wave Forces

The above-mentioned examinations confirm that the wave forces of non-breaking waves are to be given well by the following equation in considering the phase lag ε of the inertia force rather than by Eq.(2).

$$F_T(\theta) = (F_D)_{max} \sin^2\theta + (F_M)_{max} \cos(\theta - \varepsilon) \qquad (14)$$

$$(F_D)_{max} = \frac{w_o}{2g} DC_D \int_{-h}^{\eta_c} u_{max}^2 dz \qquad (15)$$

$$(F_M)_{max} = \frac{w_o}{g} \frac{\pi D^2}{4} C_M \int_{-h}^{\eta_c} \dot{u}_{max} dz \qquad (16)$$

In general, therefore, the maximum value of the total wave force $(F_T)_{max}$ cannot be given by Eq.(3).

According to Goda *et al.*, the maximum breaking wave force is formulated as:

$$F_B = (F_I)_e + (F_D)_{max} \sin^2\theta_B + (F_M)_{max} \cos\theta_B \qquad (17)$$

where $\theta_B = \sin^{-1}(1-\lambda)$.

While the impact force is assumed to occur at the instant when the vertical wave front impinges on the front of the cell in the above equation, the expressions of the drag force and the inertia force are based on the phase corresponding to the center line of the cell. Hence we must consider the phase difference of the water surface elevations between at the front of the cell and at the center line of the cell. By assuming that the wave profile can be expressed by a sinusoidal form for simplicity, this phase difference is expressed by $\delta_B = \pi D/L_b$. In addition to this phase difference, it is necessary to introduce the phase lag ε of the inertia force in order to revise Eq.(17) for the large diameter cell. Based on these considerations, the general formula of breaking waves acting on a pile or a cell is proposed as follows:

$$F_B = (F_I)_e + (F_D)_{max} \sin(\theta_B - \delta_B) |\sin(\theta_B - \delta_B)| + (F_M)_{max} \cos(\theta_B - \delta_B - \varepsilon) \qquad (18)$$

where $\delta_B = \pi D/L_b$, $\theta_B = \sin^{-1}(1-\lambda)$.

Comparison of Measured Values and Calculated Ones

The best way to examine these computation methods is to compare the measured wave forces to the computed ones. Figures 10 and 11 show this comparison for each wave period for the cases in which the cell diameter is 50 cm and 13 cm respectively. The ordinate $(F_T)_{max}$ is the maximum value of total force, the abscissa H_o means the reduced wave height in deep water, and small numbers in these figures indicate the wave height at the depth of the test cell.

The solid circles are the measured values of $(F_T)_{max}$, which are the averaged values for each sequence of wave force records. Each figure shows that as the offshore wave height H_O becomes large, the total wave force also increases first until it reaches a maximum value, and then decreases rapidly. This corresponds to the change of wave conditions from non-breaking to just-breaking, and finally to after-breaking.

According to Eq.(14), the maximum value of non-breaking wave force is not represented by Eq.(3). It is, however, reasonable to calculate $(F_T)_{max}$ by Eq.(3) under the present experimental conditions. In the case of the cell diameter of 13 cm, the phase difference ε is about 5 degrees at the most and $\sin^2\varepsilon$ is less than 0.01, and therefore the error owing to the use of Eq.(3) in computation of $(F_T)_{max}$ is less than 1 per cent. On the other hand in the case of 50 cm diameter, although the value of $\sin^2\varepsilon$ reaches 0.12, the value of $(F_D)_{max}$ is only 10 per cent of $(F_M)_{max}$, and the error due to the use of Eq.(3) is also 1 per cent at the most.

In the present analysis the computations of total forces are based on the following quantities. The inertia coefficient and the phase lag are the values given by the diffraction theory, that is Eq.(10). The drag coefficient are given by the NPL curve corresponding to the steady flow as shown in Fig. 7. The horizontal velocities under the wave crest are estimated with Eq.(8) and the values of α given in Table 3. The water particle accelerations are evaluated from the small amplitude wave theory by using the measured wave heights.

The open circles in Figs. 10 and 11 are the non-breaking wave forces computed thus by Eq.(3). The open squares and the solid triangles indicate the values of breaking wave forces computed by Eq.(17) without the phase difference, and by Eq.(18) in consideration of the phase differences, respectively.

In the range of non-breaking waves, the agreements between the measured forces and the computed ones by Eq.(3) are fairly good in both cases of the large diameter and the small diameter. As for the impulsive forces of just-breaking and immediately-after-breaking waves it is as follows. In the first cases where the cell diameter is 50 cm, the calculated values by Eq.(17), which has been proposed by Goda *et al.*, are rather small in comparison

with the observed ones. Besides they are smaller than even the values by Eq.(3), which does not include the impact force component, for wave period $T \leq 1.75$ sec. On the contrary, Eq.(18) proposed by introducing both the impact force and the phase differences gives reasonable values in this range. For $T \leq 1.5$ sec, Eq.(3) yields the best agreements with the observed values, but it cannot manifest the impulsive characteristics observed clearly in the wave force records. This result implies that it is better to use Eq.(18) rather than Eq.(3) in the range of breaking waves even for these wave periods, although it is necessary to obtain more reliable values of various coefficients used in Eq.(18).

In the next cases where the cell diameter is 13 cm, the phase differences δ_B and ε are so small that Eq.(17) and Eq.(18) give almost the same values, and these values agree well with the observed ones in the range where the measured wave forces reach their maximum. For $T=2.0$ sec the measured values of breaking wave forces are rather small in comparison with the calculated ones. This fact is supposed to be caused by the lack of the data of just-breaking wave forces in this experiments. It is necessary to accumulate much more data and to examine them.

The after-breaking wave forces could not be investigated thoroughly on account of the irregular form of their records which seems to be indicative of turbulence in the after-breaking waves, and because of scattering of wave height data. The measured values have a tendency to fall between the calculated values by Eq.(3) and by Eq.(18).

Supplements on Wave Force Records

The above-mentioned analyses are based on the averaged wave forces for each sequence of wave force records under the same condition. The maximum values of breaking wave forces have shown remarkable variations in the present experiments in the same way as the breaking wave forces on a vertical wall. Such variations are due to the fluctuations of the breaking position, the breaker height and the wave form.

Figure 12 shows one example of the histograph of breaking wave forces acting on the large diameter cell. The distribution is not Gaussian and the most probable value is less than the mean value. The maximum value reaches almost two times the minimum value. In the pres-

ent cases the histograph trends to approach Gaussian distribution as the wave period becomes short. In all cases the occurence probability of wave forces less than 1.5 times the mean value amounts to 90 to 100 per cent.

The authors have also obtained some data for the vertical distribution of the wave forces by using the partial wave force meters which are structurally similar to the total force meter and consist of eight sliced cylindrical cells. Figure 13 shows the vertical distributions of the breaking wave forces acting on the large diameter cell. In each case the maximum value occurs in the vicinity of the still water level.

CONCLUDING REMARKS

On the basis of the experimental data on the wave forces exerted on a circular cell by non-breaking waves and by breaking waves, the computation methods of wave forces and the various coefficients have been investigated. The major conclusions are as follows:

1) The phase difference between the accelerations of the water particles and the inertia forces must be considered for the estimation of the drag coefficient as well as the inertia coefficient.

2) The formula proposed in the present paper, Eq.(18), is satisfactory to calculate the impulsive breaking wave forces even on the large cell with the diameter comparable to the wave length.

There are some problems unsolved in the application of the present formula to the estimation of the actual wave forces. The first problem is how to determine the various coefficients used in this formula. The curling factor of breaking waves has not yet been formulated in the universal form as the function of breaker characteristics. The authors are not confident whether the so-called scale effect on the values of this factor is present or not. It is necessary to devote much efforts continuously to accumulate the experimental data on this factor under various conditions. Whether the scale effect exists or not is not clear at present also as to the values of the drag coefficient. But in the design of the large diameter cell-structures, it seems not so important since the drag force component is much less than the inertia force. The third problem is how to determine the impact response factor; in other words the estimation of the natural fre-

quency of the actual structures. In the actual design, not only the natural frequency of the structure itself but also that of the foundation or the ground and the effect of the connection between them are important and difficult to estimate. The expression of the phase difference δ_B in Eq.(18) seems reasonable as the first approximation but is probably too simple to formulate the complicated real phenomena. It is desirable to improve also the value of this phase difference in future.

REFERENCES

Goda, Y. (1964): "Wave forces on a vertical circular cylinder; Experiments and proposed method of wave force computation", Rept. Port and Harbour Res. Inst., Ministry of Transport, Japan, No. 8, 74 p.

Goda, Y. (1970): "A synthethis of breaker indices", Proc. Japan Soc. Civil Engrs., No. 180, pp. 39-49. (in Japanese)

Goda, Y., S. Haranaka and M. Kitahata (1966): "Study of impulsive breaking wave forces on piles", Rept. Port and Harbour Res. Inst., Ministry of Transport, Japan, Vol. 5, No. 6, 30 p. (in Japanese)

Hall, M. A. (1958): "Laboratory study of breaking wave forces on piles", Beach Erosion Board, Tech. Memo., No. 106, 24 p.

MacCamy, R. C. and R. A. Fuchs (1954): "Wave forces on piles; A diffraction theory", Beach Erosion Board, Tech. Memo., No. 69, 17 p.

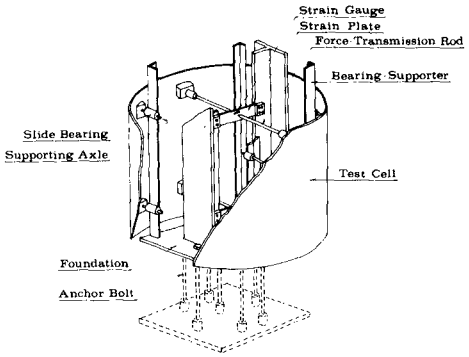

Fig. 1 Wave force measuring apparatus.

Table 1. Characteristic values of wave force meters.

Diameter (cm)	Height (cm)	Weight of Cell (kg)	Natural Frequency (Hz) in the air	in water	Sensitivity (10^{-6}strain/kg)
50	40	11.2	85	39	33
13	40	2.0	88	40	88

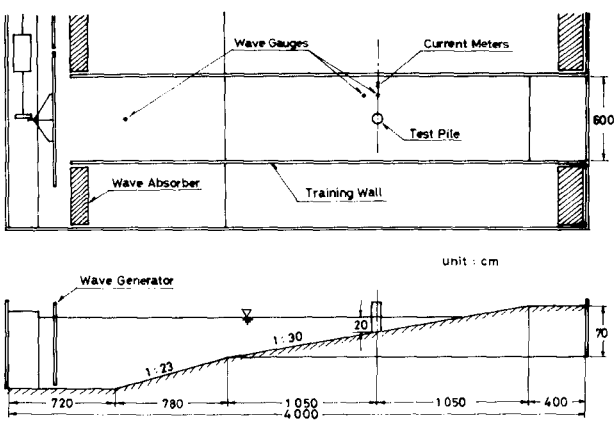

Fig. 2 Wave channel and instrumentations.

Table 2. Experimental conditions.

T (sec)	H_O (cm)	H_S (cm)	D/L D=50 cm	D=13 cm
1.00	3.0 - 13.4	2.7 - 13.1	0.35 - 0.41	0.092 - 0.110
1.25	2.6 - 14.3	2.4 - 14.5	0.26 - 0.31	0.067 - 0.080
1.50	2.7 - 17.7	2.7 - 16.0	0.20 - 0.25	0.052 - 0.064
1.75	2.2 - 17.5	2.3 - 18.2	0.16 - 0.21	0.041 - 0.055
2.00	2.4 - 19.3	2.7 - 20.1	0.14 - 0.18	0.037 - 0.048

H_O : Reduced offshore wave height
H_S : Wave height at the location of the cell
$L = cT$, c : Wave celerity measured at the location of the cell

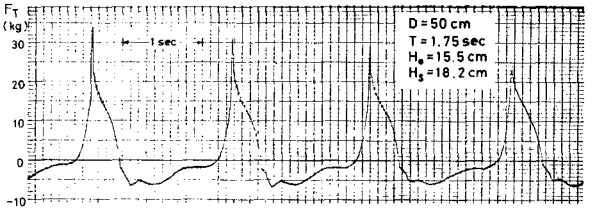

Fig. 3 Typical record of breaking wave force on a cell.

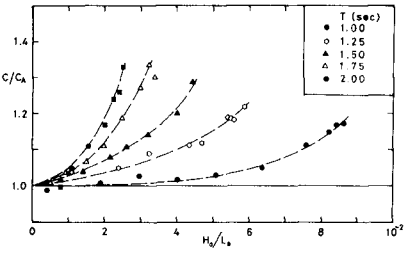

Fig. 4 Relation between wave celerity and wave steepness.

Table 3. Breaker characteristics and a factor α

T (sec)	h/L_A	H_b/h	Y_b/h	L_b/L_A	α
1.00	0.165	0.655	1.47	1.16	0.813
1.25	0.125	0.715	1.53	1.19	1.025
1.50	0.101	0.800	1.60	1.22	0.913
1.75	0.085	0.910	1.70	1.34	0.767
2.00	0.074	0.980	1.77	1.33	0.601

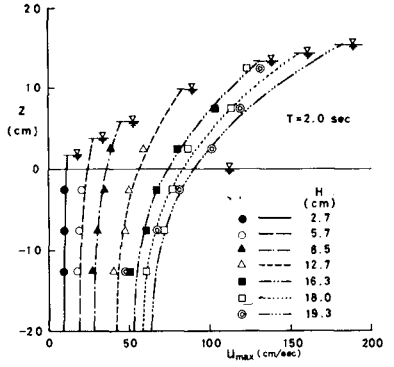

Fig. 5 Vertical distributions of horizontal velocity under wave crest.

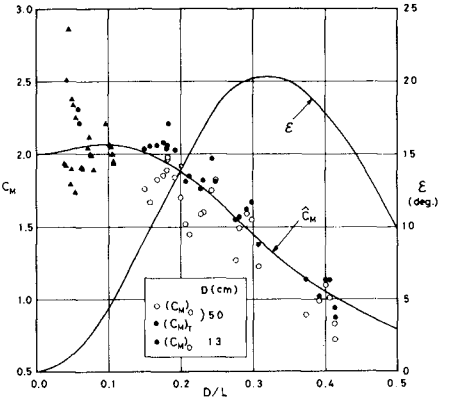

Fig. 6 Inertia coefficient and phase lag of inertia force.

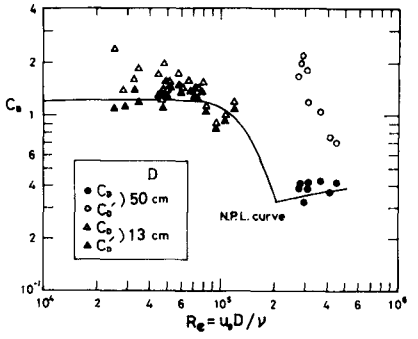

Fig. 7
Relation between drag coefficient and Reynolds number.

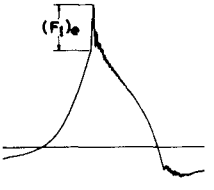

Fig. 8 Effective impact force.

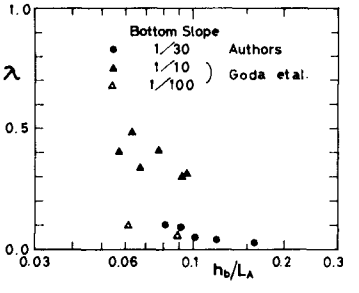

Fig. 9 Relation between curling factor and relative depth.

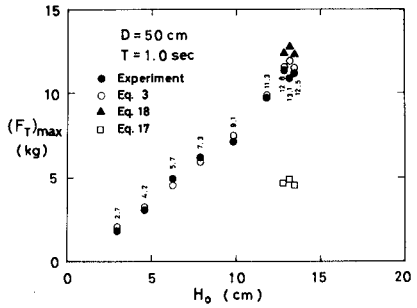

(a)

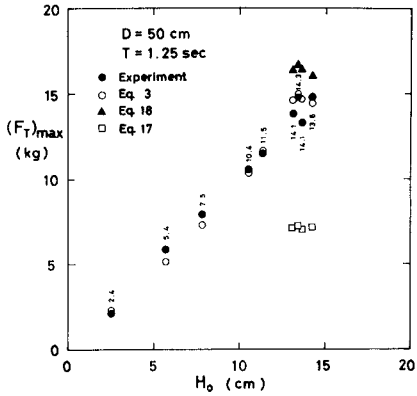

(b)

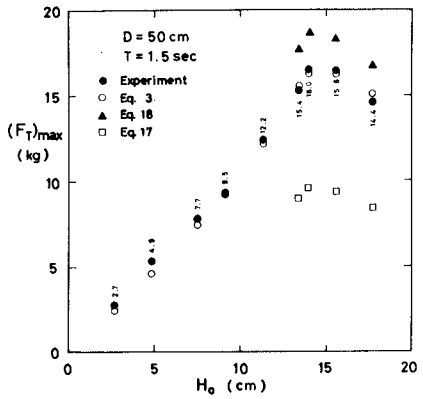

(c)

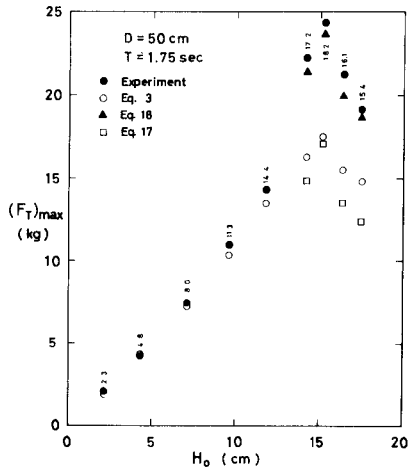

(d)

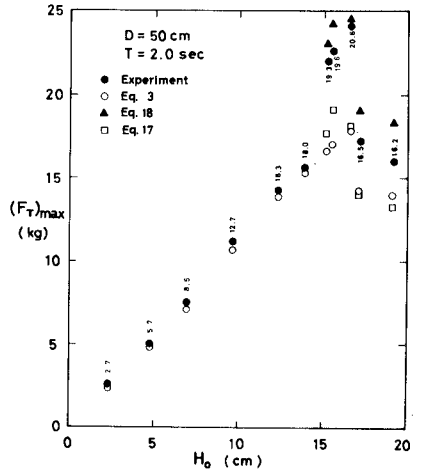

(e)

Fig. 10 Comparison of measured wave forces and calculated ones. (D = 50 cm)

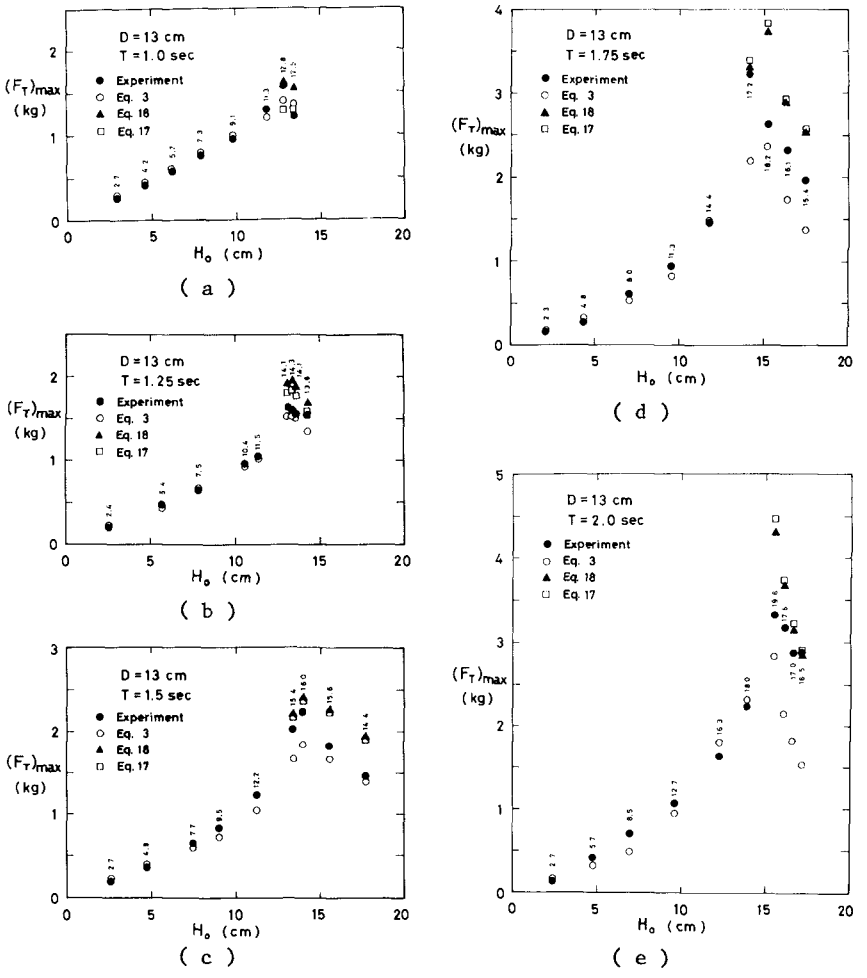

Fig. 11 Comparison of measured wave forces and calculated ones. ($D = 13$ cm)

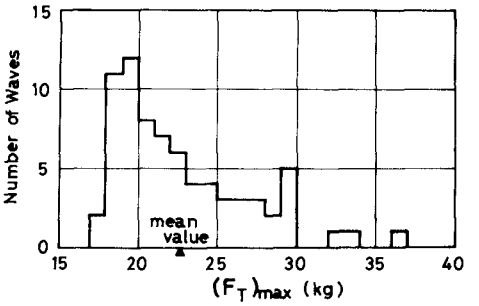

Fig. 12 Histograph of breaking wave force.
(D = 50 cm, T = 2.0 sec, H_S = 19.6 cm)

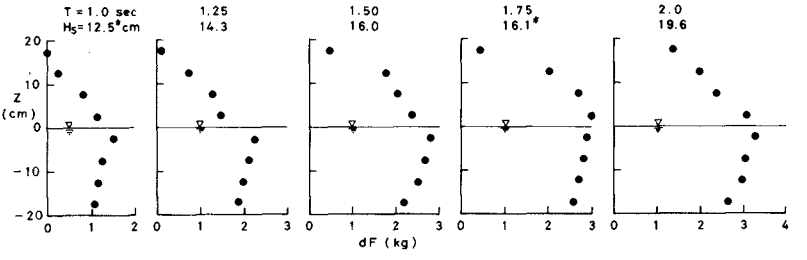

Fig. 13 Vertical distributions of breaking wave forces.
(D = 50 cm, * : after-breaking wave height)